Journal of Materials Chemistry A

Accepted Manuscript

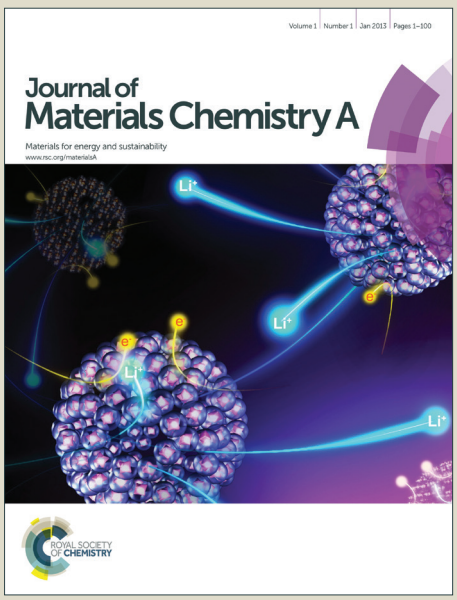

ROYAL SOCIETY OF CHEMISTRY

www.rsc.org/materialsA

Journal of Materials Chemistry A

ARTICLE

Effect of Pyrolysis Pressure on Activity of Fe-N-C Catalysts for Oxygen Reduction

Received 00th January 20xx,
Accepted 00th January 20xx

DOI: 10.1039/x0xx00000x

www.rsc.org/

Cenk Gumeci,[a,c*] Nathaniel Leonard,[a] Yuanchao Liu,[a] Samuel McKinney,[b] Barr Halevi,[b] and Scott Calabrese Barton[a*]

Iron and nitrogen doped carbon, Fe-N-C, catalysts are synthesized by high pressure pyrolysis of Ketjenblack carbon, melamine and iron acetate precursor mixture in a closed, reusable scale-up stainless steel reactor. The effects of precursor loading with constant precursor ratios on obtained pressure, nitrogen retention and oxygen reduction reaction (ORR) activities are studied. The results indicate that higher precursor loading increases the gas phase pressure and improves nitrogen retention and ORR activity. Furthermore, a relationship is found between active site density, nitrogen retention and pressure that suggests that the limiting reaction may be an adsorption process driven via high pressure of volatile intermediates from the melamine.

1. Introduction

Platinum (Pt) and Pt-based materials are the most effective oxygen reduction reaction (ORR) catalysts in proton exchange membrane fuel cells (PEMFCs).[1] Due to their high cost and scarcity, wide commercialization of PEMFCs is still limited.[1] Consequently, replacing these catalysts with non-precious materials has gained accelerating attention in the past few decades.[2,3] Among them, metal-nitrogen doped carbon catalysts, commonly abbreviated as MNC where M = Co, Fe, Mn etc. have proven to be the most active non-precious ORR catalysts in acidic medium.[4,5,6,7] MNC catalysts are typically prepared by the pyrolysis of a variety of transition metal salts (such as sulfates, nitrates, acetates and chlorides), nitrogen precursors (such as acetonitrile, aniline, melamine etc.) and carbon support (such as Vulcan XC-72, Ketjenblack, Black Pearls etc.) materials.[3] Since Yeager's pioneering study on the preparation of MNC catalysts in 1989,[8] many methods have been developed to prepare MNC catalysts via varying the precursor materials.[3,9] A common feature of the most methodologies is one (or multiple) pyrolysis steps at atmospheric pressure under nitrogen or ammonia.[3,9] Plenty of studies have shown that the choice of the precursor and support and synthesis conditions such as heat treatment temperature and atmosphere, post treatment conditions significantly influence ORR activity and durability of MNC catalysts.[2,3,9]

Of all metal precursors, Fe-doped MNC catalysts have so far shown the highest activity and durability in acid.[4-5,6,7,10,11] There are currently several methods to synthesize Fe-doped MNC materials, including pyrolysis of iron macrocycles, heat treatment of mixtures of iron precursors and separate carbon and nitrogen sources,[2-3] including a high loading of nitrogen precursor to form self-supported catalysts.[7,12,13,14] While these MNC catalysts show promise as a replacement for Pt, the knowledge on the exact nature and formation of catalytic active sites, along with the mechanism of oxygen reduction are still limited. This is mostly due to the use of inherently uncontrolled pyrolysis.

In our previous studies, high pressure pyrolysis (HPP) in the absence of inert gas was adopted to synthesize Fe-doped MNC catalysts.[15,16,17,18] This approach was designed to increase the density of nitrogen-based active sites because of the improved equilibrium conditions that occur at high pressures. We also demonstrated that the choice of nitrogen precursor, carbon support and the amount of iron precursor directly affect the ORR activity.[15,16,17,18] Flame-sealed quartz ampoules with constant volumes were used as reactors that limits the loading amount of precursors below 1 g.[15,16,17,18,19] There are several issues with the usage of ampoules, such as weakness of quartz ampoules at high temperature and pressure, the complexity of loading and sealing, inability to analyze pyrolysis pressure and scale-up, and limited batch size. In the present study, in order to overcome above mentioned issues and monitor real time pressure, a stainless steel reusable vessel reactor with an attached pressure gauge was used.

The main incentive for the present work is to investigate and explain the effect of loading (mass/volume) of precursor materials in the pyrolysis reactor, which directly impacts pyrolysis pressure and ORR activity. Fe doped MNC catalysts

[a] Department of Chemical Engineering and Materials Science, Michigan State University, East Lansing, MI 48824, United States. E-mail: cenk.gumeci@nissan-usa.com; scb@msu.edu
[b] Pajarito Powder, LLC, Albuquerque, NM 87102, United States
[c] Current address: Nissan Technical Center North America, Farmington Hills, MI 48331, United States

Electronic Supplementary Information (ESI) available: TEM image of Fe-N-C, RRDE, SWV and durability measurements. See DOI:

were synthesized by pyrolyzing a mixture of metal salt (iron acetate), nitrogen precursor (melamine) and high surface area carbon (Ketjenblack) in the reactor. Prepared catalysts, abbreviated as Fe-N-C were characterized by a combination of physical and electrochemical methods. Structural properties were evaluated by X-ray diffraction (XRD), Raman and transmission electron microscopy techniques. The ORR activity, and kinetic properties were obtained from rotating disc electrode measurements. The catalyst site density was estimated by square wave voltammetry (SWV), which allows the observation of metal oxidation-reduction couples. The Fe-N-C samples were further assayed in fuel cell membrane electrode assemblies (MEAs).

2. Experimental

2.1 Materials and Reagents

Iron (II) acetate, persulfonic acid copolymer (5 wt %) and melamine were obtained from Alfa Aeser (Ward Hill, MA). High surface area carbon, Ketjenblack 600 JD, was purchased from Akzo Nobel (Chicago, IL). Carbon supported Pt (Pt-C, 40 wt%) was purchased from Alfa Aeser (Ward Hill, MA). Nitrogen and oxygen gases (Air Gas, Lansing, MI) were of ultrahigh purity. ACS grade sulfuric acid was used. All aqueous solutions were prepared with deionized water (~18 MΩ-cm) from a four-cartridge Barnstead Nanopure Infinity D4741 (Thermo Scientific). 200 proof ethanol was obtained from Koptec (King of Prussia, PA).

2.2 Synthesis of Fe-N-C Catalysts

Catalysts were synthesized as described previously.[15,16,18] In a typical synthesis, ethanol cleaned Ketjenblack (95.7 wt %), melamine (0.8 wt %) and iron (II) acetate (2.2 wt %) were dispersed in absolute ethanol and dried overnight at 80°C. Obtained dry powder then were mixed with melamine in a ratio of 5:9 (melamine: dry powder) to achieve nitrogen content of 24 wt %.[16] A desired amount of mixture (0.48, 0.75, 2.4 and 3.5 g) was inserted in a quartz reaction tube (Fig. 1a) with a quartz rod inserted to reduce the available reactor volume from 100 mL to 17.5 mL. The reaction tube then was inserted in a home-made, stainless steel reactor attached with an analog pressure gauge as shown in Fig. 1a. The pyrolysis temperature was fixed at 800°C for 3 hours.

2.3 Structural Characterization

Catalyst surface area was analyzed using a Micrometrics ASAP 2020 Physisorption Analyzer. Nitrogen adsorption isotherms at 77 K were collected. The Brunauer, Emmett and Teller (BET) surface area calculation[20] was used to analyze isotherms. Pore size distribution was calculated by density functional theory (DFT)21 assuming a slit pore geometry for pores. X-ray diffraction (XRD) patterns were collected at 40 kV and 44 mA using Bruker AXS Model D8 using Ni filtered Cu-Kα radiation (λ= 1.54Å). Scans were recorded in the 2θ range of 10-80°. Raman spectra were obtained using a Horiba Aramis Raman confocal microscope. Transmission electron microscopy (TEM) images were obtained using a JOEL 2200FS at 200 kV equipped with an energy dispersive X-ray (EDX) spectrometer. Samples were mounted by suspending a small amount of the dried sample in ethanol, dispersing a low-power ultrasonic bath and then placing two drops onto an ultrathin silicon monoxide formvar grid (Ted Pella). Carbon hydrogen nitrogen (CHN) analysis were performed by Midwest Microlab (Indianapolis, IN).

2.4 Electrochemical Characterization

Electrochemical studies were conducted in a conventional three-electrode glass cell using a potentiostat (Bio-Logic SA) and a rotating disc assembly (Pine Research Instruments, Raleigh, NC). A glassy carbon disc electrode (Pine Research Instrument, 5 mm diameter) was used as the working electrode while a Pt wire served as a counter electrode. It should be noted that Pt wire is stable in the potential region that is being studied and safe to use as the counter electrode.[7] We did not observe any Pt features on cyclic voltammetry of MNC in nitrogen saturated sulfuric acid electrolyte (See supporting Fig. 1). A home-made reversible hydrogen electrode (RHE) was used as a reference electrode.[22,23]

Prior to each experiment, a glassy carbon electrode was polished to a mirror finish using a 0.05 µm alumina suspension, followed by rinsing with ultrapure water to remove alumina particles from the surface. Fe-N-C catalyst ink was prepared by ultrasonically (Misonix, Sonicator 3000) mixing 4 mg of catalyst powder in 150 µL ethanol and 50 µL ionomer (5 wt %). The catalyst suspension was dispensed on the glassy carbon electrode in a 5 µL aliquot to yield the loading of 0.5 mg $cm^{-2}_{(geo)}$. Similarly, 5 mg of Pt-C (40% wt Pt) was mixed in 3 mL of ethanol, 1 mL of water and 0.1 mL of ionomer solution. Followed by sonication, a 10 µL aliquot was dispensed on to the glassy carbon electrode to yield the loading of ~ 25 μg_{Pt} $cm^{-2}_{(geo)}$.

Electrochemical experiments were conducted in either nitrogen or oxygen saturated 0.5 M sulfuric acid solution at room temperature. The open circuit potential of the electrode was monitored until stabilized. Linear sweep voltammograms (LSVs) were obtained in the potential range of 0.2 – 1 V (RHE) at a scan rate of 0.5 mV s^{-1}. The electrochemical durability study performed on best performing catalyst in O_2 saturated 0.1 M H_2SO_4 with a 900 rpm rotating rate and a 50 mVs^{-1} scan rate for 1000 cycles in the range of 0.2 – 1 V (RHE).

2.5 MEA Preparation and Fuel Cell Test

Membrane electrode assemblies (MEAs, 5 cm^2) were made from gas diffusion electrodes pressed onto 211 Nafion® membrane with PTFE-impregnated glass-fiber sub-gaskets at 131°C for 10 minutes at 90 psi, then allowed to cool under 1 psi pressure. Sub-gasket thickness for the anode was 150 micrometer and 250 micrometer for the cathode, respectively. The gas diffusion electrodes were sprayed using Sono-tek Exacta-Coat automated spray system with a 25 kHz ultrasonic nozzle onto SGL 25BC gas diffusion layer materials heated to

65°C. Ink was deposited in a rate of 40 µg cm^{-2} per deposition pass, for a total of 3 $mg_{catalyst}$ cm^{-2}. The ink was composed of 4 mL Isopropyl Alcohol, 2 mL deionized water, 200 mg of catalyst mixed with 300 mgs D2021 Nafion® dispersion. A 50 mL vessel containing the ink ingredients was placed in a water bath and mixed for 30 minutes using an IKA T-18 high-shear mixer with S18-19G dispersing element set for 18000 rpm.

The MEAs were loaded into the cell testing assembly (Fuel Cell Technologies, Albuquerque, NM) with single serpentine-pattern graphite flow plates and the cell hardware was assembled using 4.5 N-m torque. The cell was allowed to come up to temperature under a 200 sccm feed of 100% RH Air and H_2 and pressurized to a total of 1.8 Atm total pressure. After cell temperature reached 80°C, load was applied potentiostatically to 0.3 V for 10 minutes. Sequential polarization curves were measured with current measurement after a 60 second hold at each potential. When changing between gasses, 30 minutes was used to allow to system to stabilize before additional measurements.

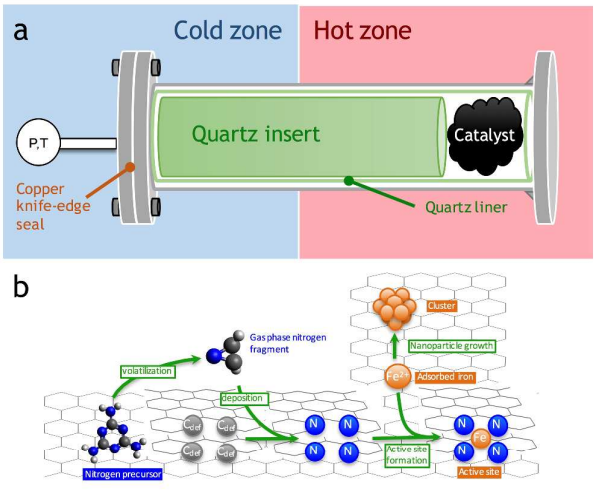

Figure 1. a) Schematic diagram of the reactor and **b)** proposed reaction mechanism.

3. Results and Discussion

3.1 Synthesis

In this study, a large, stainless steel reactor was used to sustain high temperature and pressure. Figure 1 a-b shows the schematic illustration of the reactor and possible reaction mechanism, respectively. Based on our previous experience, the ratios of iron acetate, Ketjenblack and melamine are kept constant.[15,16,17,18,24] Nitrogen and iron content is thereby fixed at ~ 24 and 1 % wt, respectively. Pyrolysis at 700-1000 °C usually enhances the activity and durability of a MNC catalyst and a proper temperature will result in higher activity. Based on our previous work,[15,16,18,24] 800 °C is chosen as the optimum pyrolysis temperature for HPP synthesis of Fe-N-C. The dried precursor mixture is placed in a quartz reaction tube followed by the insertion of a quartz rod (Fig. 1a). The rod reduces the available reactor volume from 100 mL to ~ 17.5 mL. The precursor density in the reactor ranges from 27 mg cm^{-3} to 200 mg cm-3 (See Table 1). This compares to a density of 50 mg cm^{-3} for previous studies using quartz ampoules.[15,16,18,24] The quartz tube also protects the catalyst precursor from contamination by the stainless steel reactor wall. The reactor was designed with two different temperature zones: a hot zone for Fe-N-C pyrolysis and a cold zone for sealing and pressure control. In order to monitor autogenic pressure, an analog pressure gauge was attached at the low temperature zone.

During the synthesis, autogenic pressure is generated due to decomposition and evaporation of melamine and acetate (from iron acetate). Retention of volatile intermediates leads to increased nitrogen content and site density. In Fig. 1b, we propose a possible mechanism for the active site formation which includes volatilization of melamine, followed by adsorption of the precursors at carbon defects (Fig. 1b). This allows subsequent complexation with mobile surface iron species. Side reactions include metal nanoparticle formation that can lead to additional side reactions (such as carbon nanotube formation catalyzed by iron) if the iron content is high enough. Previously we observed the appearance of iron nanoparticles at loadings of iron acetate 3 wt% or more.[18] The maximum pressure is obtained at the second half of the pyrolysis and stays constant at the end of 3-hour HPP at 800 °C. As expected, higher loading of precursor increases the autogenic pressure thus positively affects the nitrogen retention. As shown in Table 1, there is an obvious correlation with precursor loading, maximum pressure and nitrogen retention. Higher nitrogen retention often leads a superior

Table 1. Fe-N-C Catalyst Properties

Precursor Loading (g)	Precursor Density (mg cm^{-3})	Yield (%)	Pressure* (psi)	N Content† (wt %)	Surface Area (m^2 g^{-1})	I_D/I_G‡	Current Density# (mA cm^{-2})
0.48	27	56	45	2.45 ± 0.05	1215	1.64	0.31
0.75	43	60	65	3.50 ± 0.08	1297	1.53	0.53
2.4	137	67	170	6.54 ± 0.24	1109	1.48	0.88
3.5	200	73	280	7.03 ± 0.03	1137	1.33	1.1

*Max pressure obtained in the second half of pyrolysis (1.5 hour after the temperature reaches 800 °C). † Obtained from CHN analysis with error estimated from standard deviation of three distinct experiments. ‡Estimated from Raman spectra in Fig. 4. #Derived from polarization curves in Fig. 5 at 0.8 V.

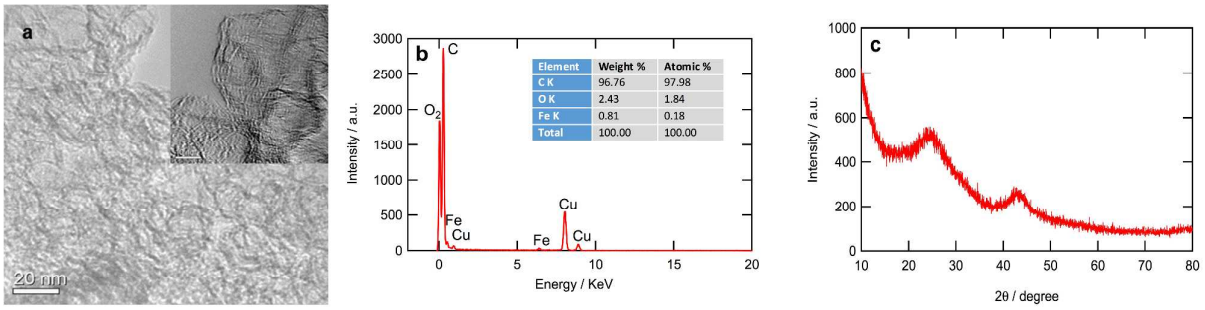

Figure 2. a) Representative TEM images of Fe-N-C, (3.5 g Batch), the scale bar inset: 10 nm; **b)** corresponding EDX, copper signal arises from copper TEM grid and **c)** XRD

ORR activity (see below for detail). However, there is still not a concrete agreement on catalytic efficiency of different nitrogen functionalities and the role of the metal in MNC catalysts.[10,13,25,26,27]

3.2 Physical Characterization

Fig. 2a presents representative TEM images of Fe-N-C catalyst (3.5 g batch). As shown in the Fig. 2a there is no obvious nanoparticle formation. This is mainly due to well distributed Fe-N sites on the catalyst which could provide a segregation between free iron ions, and as a result prevents the aggregation and formation of iron nanoparticles.[18] We recently observed that the presence of iron nanoparticles on Fe-N-C catalysts adversely affects the ORR kinetics.[18] Additionally, the high resolution TEM image (Fig. 2a inset) indicates the crystallinity of the Fe-N-C. EDX analysis (Fig. 2b), indicates that iron content is close to the nominal value of 1 wt%. In the XRD measurement (Fig. 2b), patterns obtained for Fe-N-C (3.5 g batch) display two diffraction peaks, corresponding to (200) plane for carbon at $2\theta \approx 26°$ and a diffraction peak at $2\theta \approx 44°$ attributable to the combination peak of iron nitride and carbide.[28,29] XRD analysis also proves the absence of iron oxide, iron hydroxide and metallic iron species.[28,29,30]

High surface area and optimum mesoporosity are key requirements for highly active MNC catalysts for ORR. In this study, high surface area carbon, Ketjenblack, was used as thesupport. As shown in the Fig. 3, Ketjen and Fe-N-C catalysts both exhibited Type IV (IUPAC) isotherms.[31] The calculated BET surface area values for Fe-N-C catalysts are lower that of Ketjenblack (~ 1420 $m^2 g^{-1}$) and microporosity of the catalysts decreases after HPP (see Table 1). This is mainly due to the decomposition products of melamine that can deposit on the surface at the high temperature and pressure which also leads a slight increase in the micropore sizes.[15] In general, surface areas among the Fe-N-C samples also slightly vary with respect to loading. The pore mode observed above 20 nm is increased from ~ 22 nm for Ketjenblack to ~ 40 nm for the catalysts, possibly due to combined effects of high pressure and the etching capability of ammonia generated during HPP. The ammonia gas intermediate can etch non-graphitic carbon, increasing mesoporous surface area and accessible active site density for ORR.[4] As shown in the Fig. 3b, Fe-N-C As shown in the Fig. 3b, Fe-N-C catalysts have larger pores (above 20 nm) than that of Ketjenblack which is in good agreement with the TEM observation(See supporting Fig. 2). HPP could create random larger pores inside of the Fe-N-C matrix.

Fig. 4 presents Raman spectra for the Fe-N-C samples and Ketjenblack. Two bands observed at ~1350 cm^{-1} and at ~1580 cm^{-1} are the D band (disorder vibration mode) and G band (also known graphitic carbon).[32] The relative presence of the amorphous carbon with respect to graphitic carbon can be estimated from the intensity ratio between the D and G bands.[32] Normally, in the presence of heteroatoms on carbon, defect density increases, resulting in a higher I_D/I_G ratio.[32] Surprisingly, I_D/I_G ratio of the catalysis samples (Table 1) are lower than that of Ketjenblack (I_D/I_G=3.48) and tend to decrease slightly as a function of loading, indicating improved graphitization at higher pressure / loading.

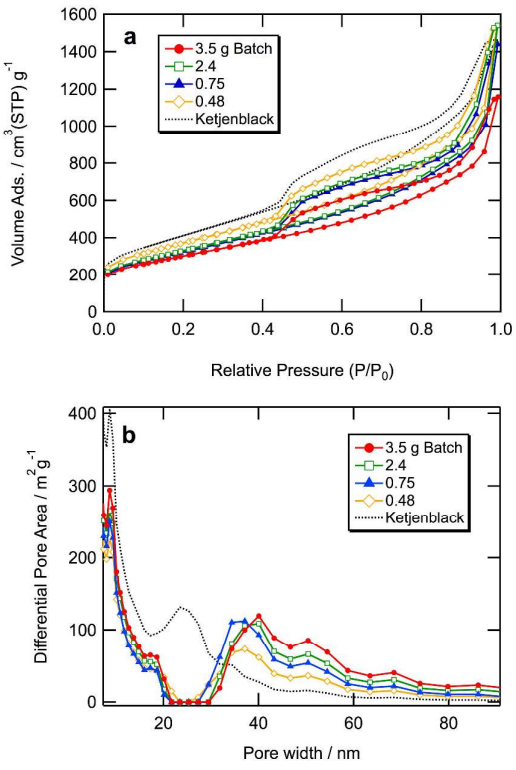

Figure 3. a) Nitrogen adsorption-desorption isotherms and **b)** corresponding pore-size distribution plots.

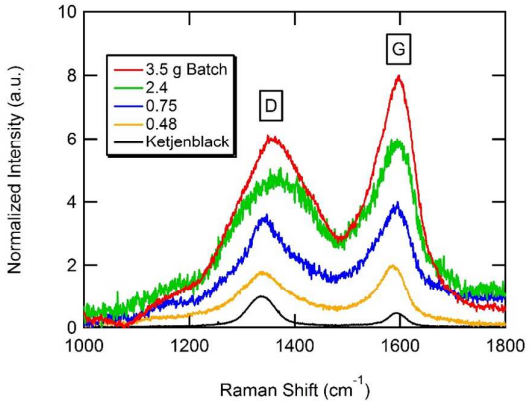

Figure 4. Raman spectra for the Fe-N-C samples and Ketjenblack.

3.3 Electrochemical Characterization

ORR activity of each catalyst were screened with a RRDE assembly in oxygen-saturated sulfuric acid electrolyte. Fig. 5 reports the results of set of polarization curves for Fe-N-C catalysts and commercially available Pt-C (40 wt%). According to Fig. 5, half-wave potential ($E_{1/2}$) of Pt-C is shifted towards positive voltage (by as much as ~100 mV), indicating that it has superior ORR activity compared to Fe-N-C catalysts. The polarization data show that the onset potential of ORR for the higher loading samples are higher in the case of the Fe-N-C catalysts. In order to quantify ORR activity, specific current density were determined at 0.8 V from the polarization curves in Fig. 5. The obtained activities (Table 1) range from 0.32 to 1.1 mA cm^{-2} compared to 2.8 mA cm^{-2} for Pt-C, respectively. The results are comparable to other Fe-N-C catalysts investigated recently in similar conditions.[18,19,33,34,35,36] All LSVs were obtained at a 0.5 mV s^{-1} scan rate. Such a slow scan eliminates capacitive background current without additional corrections.

We also note that diffusion current density values are also slightly increased for higher precursor loading samples. As expected, the higher precursor loading also improves ORR performance (Fig. 5b). The calculated kinetic current densities are also higher for higher loading Fe-N-C catalysts (See supporting Table S1). We attribute this effect to increased gas-phase nitrogen activity driving increased Fe-N active site density. In Fig. 5b, a linear relationship is clearly observed between loading amount, nitrogen content and ORR activity. Since, the loading amount of Fe precursor is constant for all samples, higher nitrogen content likely enhances the number of Fe-N active sites. For evaluation of the ORR selectivity, a rotating ring disc electrode study performed on Fe-N-C catalyst (3.5 g Batch) that indicates ORR proceeds primarily through the direct 4 e^- pathway to water (See supporting Fig. S3 for details) which corroborates well with our recent work.[24]

In order to elucidate the active sites of the Fe-N-C catalysts, square wave voltammetry was performed in nitrogen saturated 0.5 M H_2SO_4 electrolyte, to detect faradaic redox couples while minimizing capacitive current.[13,26] As shown in the Fig. 6, all catalysts exhibit an anodic redox peak

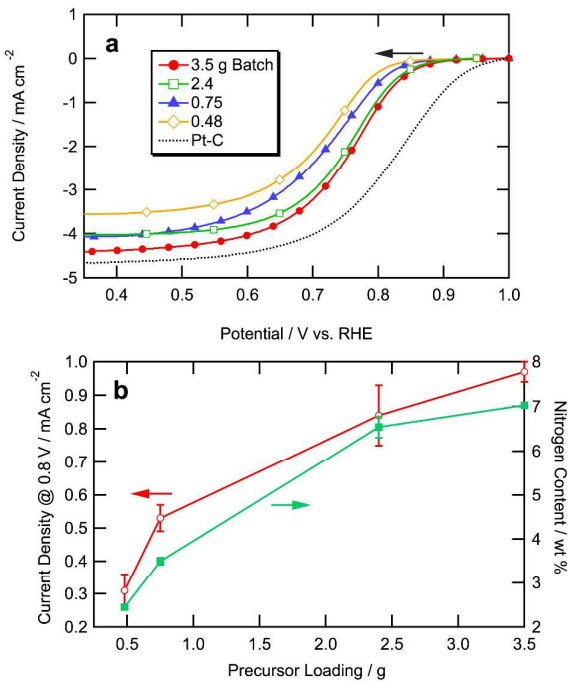

Figure 5. a) Linear sweep voltammograms (LSVs) for Fe-N-Cs and Pt –C were obtained in room-temperature, oxygen saturated 0.5 M H_2SO_4 with a 1200 rpm rotating speed at a 0.5 mV s^{-1} scan rate in negative direction (see arrow) and **b)** loading-nitrogen content-current density relationships. The current densities are obtained at 0.8 V. Error bars represents standard deviations of at least 3 different measurements.

near 0.7 V (RHE) attributable to Fe^{2+}/Fe^{3+}.[13,26,27] In comparison, oxidized carbon materials might display a peak at 0.6 V in acid, associated with the hydroquinone / quinone redox couple.[37] Indeed, the obtained SWV for Ketjenblack is flat. Additionally, there is no apparent one-electron redox transition (outer sphere electron transfer) involving the delocalized π e^- in the macrocyclic system which is observed above 1.2 V[26] (See supporting Fig. S4). This transfer mechanism tends to promote 2 e^- reduction of oxygen to peroxide in acidic medium.[26,27] It has been shown that Fe centers coordinated to nitrogen groups (mainly Fe-N_4) on carbon surfaces constitute the active sites for ORR.[13,14] Fe-N_4-C active site density may then be calculated by integrating the SWV profiles.[26,27] As shown in Fig. 6b, electrochemically estimated Fe-N-C active site density linearly correlates with current density and loading amounts, reinforcing the idea that the iron redox couple is associated with active site density

In order to test ORR activities of Fe-N-C catalysts in a running fuel cell environment, 5 cm^2 single-cell MEAs prepared with catalysts at the cathode were tested. For each MEAs prepared, there is a complex relation between MNC catalysts and ionomer (often Nafion®) affecting the overall performance of the fuel cell.[38,39] It has been shown that ~ 50 wt % Nafion® resulted in optimum MEA performance for non-PGM catalysts.[39] In this study 55 wt % Nafion® content was used in

order to improve kinetic performance via better ionic transport and conductivity in MEAs.

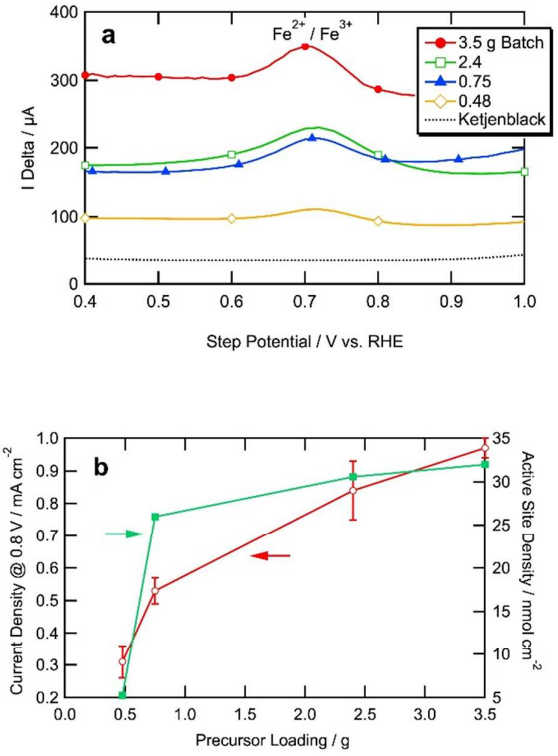

Figure 6. a) Square wave-voltammetry (SWV) profiles of Fe-N-C samples and Ketjenblack in nitrogen saturated 0.5 M H_2SO_4. All SWV experiments were performed with a step potential of 5 mV, amplitude of 20 mV, and frequency of 10 Hz, **b**) active site-current density-loading relationship.

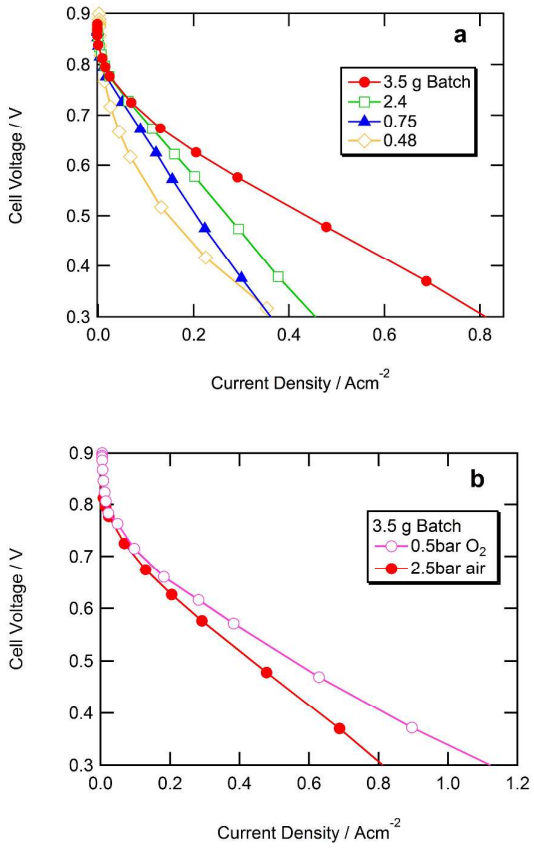

Figure 7. a) Fuel cell polarization curves of Fe-N-C samples obtained in a single cell (5 cm^2) on air with 2.5 bar back pressure. The loadings are 2.4–3.2 mg cm^{-2} and normalized to 3 mg cm^{-2} and **b)** fuel cell polarization curves of 3.5 g Batch with 2.5 back pressure in air and 0.5 bar backpressure in O_2. The loadings are 3 mg cm^{-2}. Polarization curves were obtained at 100% RH using 211 Nafion®, 55 wt% 1100 EW and 25BC GDL.

Fig. 7a. illustrates I-V performance curves of the MEAs prepared Fe-N-C catalysts. In general, the obtained performances for Fe-N-C samples are in good agreement with the results obtained from RDE experiments in both kinetic region and mass transport region. For example at 0.7 V, the catalysts have current densities of ~ 0.03, 0.05, 0.06 and 0.1 A cm^{-2} for 0.48, 0.75, 2.4 and 3.5 g batch samples, respectively. The obtained result from best performing Fe-N-C are comparable to those recently published Fe-N-C catalysts prepared by high pressure pyrolysis[19] and reactive ball-milling methods[39]. We also studied the 3.5 g batch for transport limitation using 0.5 bar O_2 and 2.5 bar air, as shown in the Fig. 7b. The current density reached 1 A cm^{-2} in oxygen and 0.68 A cm^{-2} in air, comparable to recently reported studies, but at 1+ gram per batch scale.[19,39,40,41] It should be also noted that all I-V curves were obtained without IR correction. This performance is promising and does not reflect the full potential of the catalysts in MEA form since electrode structure was not optimized.

The durability of the best performing catalyst (3.5 g Batch) was also examined in oxygen-saturated sulfuric acid solution.[7] Even in such a harsh durability test, the half-wave potential of the aged catalyst is shifted no more than 30 mV (see supporting Fig. S5). Ongoing effort focuses on the improving activity and durability of these Fe-N-C catalysts.

4. Conclusions

High pressure pyrolysis using a large reactor was shown to be effective in assisting the preparation of Fe-N-C ORR catalysts for scale-up synthesis. In the synthesis, an economical nitrogen rich precursor, melamine, Ketjenblack and iron acetate mixture was pyrolyzed in a closed stainless steel reactor without purging any gas. Precursor loading and its effect on autogenic pressure played an important role in improving ORR activity due to formation of iron-nitrogen active sites. Active site density, determined by square wave voltammetry, increased as a function of precursor loading. The best ORR catalyst was obtained from the highest precursor loading sample (3.5 g Batch) with had highest nitrogen content (~7 at. %) and Fe-N active site density. Furthermore, the Fe-N-C

catalyst predominantly reduces oxygen to water by a 4 e^- process that is a possible inner-sphere electron transfer reaction with no more than 3.5 % H_2O_2 generation. MEA studies revealed that the performance of these Fe-N-C catalysts is comparable in recent literature in operating fuel cells. Further optimization studies are required to be completed to improve the fuel cell performance and durability.

5. Acknowledgements

We gratefully acknowledge the partial financial support from the U.S. Department of Energy (EERE), under a Non PGM Catalyst development effort (Contract no EE 0000459) lead by Northeastern University (Prof. Sanjeev Mukerjee, P.I).

6. References

1 M. K. Debe, *Nature*, 2012, **486**, 43.
2 F. Jaouen, E. Proietti, M. Lefèvre, R. Chenitz, J.-P. Dodelet, G. Wu, H. T. Chung, C. M. Johnston and P. Zelenay, *Energy Environ. Sci.*, 2011, **4**, 114.
3 G. Wu and P. Zelenay, *Acc. Chem. Res.*, 2013, **46**, 1878.
4 M. Lefèvre, E. Proietti, F. Jaouen and J.-P. Dodelet, *Science*, 2009, **324**, 71.
5 G. Wu, K. L. More, P. Xu, H.-L. Wang, M. Ferrandon, A. J. Kropf, D. J. Myers, S. Ma, C. M. Johnston and P. Zelenay, *Chem. Commun.*, 2013, **49**, 3291.
6 R. Bashyam and P. Zelenay, *Nature*, 2006, **443**, 63.
7 A. Serov, K. Artyushkova and P. Atanassov, *Adv. Energy Mater.*, 2014, **4**, 1.
8 S. Gupta, D. Tryk, I. Bae, W. Aldred and E. Yeager, *J. Appl. Electrochem.*, 1989, **19**, 19.
9 Z. Chen, D. Higgins, A. Yu, L. Zhang and J. Zhang, *Energy Environ. Sci.*, 2011, **4**, 3167.
10 K. Strickland, E. Miner, Q. Jia, U. Tylus, N. Ramaswamy, W. Liang, M.-T. Sougrati, F. Jaouen and S. Mukerjee, *Nat. Commun.*, 2015, **6**, 7343.
11 F. Jaouen, J. Herranz, M. Lefévre, J. P. Dodelet, U. I. Kramm, I. Herrmann, P. Bogdanoff, J. Maruyama, T. Nagaoka, A. Garsuch, J. R. Dahn, T. Olson, S. Pylypenko, P. Atanassov and E. a. Ustinov, *ACS Appl. Mater. Interfaces*, 2009, **1**, 1623.
12 A. Serov, M. H. Robson, K. Artyushkova and P. Atanassov, *Appl. Catal. B Environ.*, 2012, **127**, 300.
13 U. Tylus, Q. Jia, K. Strickland, N. Ramaswamy, A. Serov, P. Atanassov and S. Mukerjee, *J. Phys. Chem. C*, 2014, **118**, 8999.
14 A. Serov, U. Tylus, K. Artyushkova, S. Mukerjee and P. Atanassov, *Appl. Catal. B Environ.*, 2014, **150-151**, 179.
15 R. Kothandaraman, V. Nallathambi, K. Artyushkova and S. C. Barton, *Appl. Catal. B Environ.*, 2009, **92**, 209.
16 V. Nallathambi, N. Leonard, R. Kothandaraman and S. Calabrese Barton, *Electrochem. Solid State Lett.*, 2011, **14**, B55 .
17 N. Leonard, V. Nallathambi and S. C. Barton, *J. Electrochem. Soc.*, 2013, **160**, F788.
18 S. Ganesan, N. Leonard and S. C. Barton, *Phys. Chem. Chem. Phys.*, 2014, **16**, 4576.
19 K. M. Palanivelu, V. Prabhakaran, V. K. Ramani and K. Ramanujam, *J. Electrochem. Soc.*, 2015, **162**, F475.
20 S. Brunauer, P. H. Emmett and E. Teller, *J. Am. Chem. Soc.*, 1938, **60**, 309.
21 C. Lastoskie, K. E. Gubbins and N. Quirke, *Langmuir*, 1993, **9**, 2693.
22 C. Gumeci, D. U. Cearnaigh, D. J. Casadonte and C. Korzeniewski, *J. Mater. Chem. A*, 2013, **1**, 2322.
23 C. Gumeci, A. Marathe, R. L. Behrens, J. Chaudhuri and C. Korzeniewski, *J. Phys. Chem. C*, 2014, **118**, 14433.
24 N. D. Leonard and S. C. Barton, *J. Electrochem. Soc.*, 2014, **161**, H3100.
25 U. I. Kramm, M. Lefèvre, N. Larouche, D. Schmeisser and J. P. Dodelet, *J. Am. Chem. Soc.*, 2014, **136**, 978.
26 N. Ramaswamy and S. Mukerjee, *Adv. Phys. Chem.*, 2012, **2012**.
27 N. Ramaswamy, U. Tylus, Q. Jia and S. Mukerjee, *J. Am. Chem. Soc.*, 2013, **135**, 15443.
28 H. Peng, Z. Mo, S. Liao, H. Liang, L. Yang, F. Luo, H. Song, Y. Zhong and B. Zhang, *Sci. Rep.*, 2013, **3**, 1765.
29 Y. Zhang, W.-J. Jiang, L. Guo, X. Zhang, J.-S. Hu, Z. Wei and L.-J. Wan, *ACS Appl. Mater. Interfaces*, 2015, **7**, 11508.
30 B. Zhao, Y. Zheng, F. Ye, X. Deng, X. Xu, M. Liu and Z. Shao, *ACS Appl. Mater. Interfaces*, 2015, **7**, 14446.
31 K. S. W. Sing, D. H. Everett, R. a. W. Haul, L. Moscou, R. a. Pierotti, J. Rouquérol and T. Siemieniewska, *Pure Appl. Chem.*, 1985, **57**, 603.
32 M. S. Dresselhaus, a. Jorio and R. Saito, *Annu. Rev. Condens. Matter Phys.*, 2010, **1**, 89.
33 D. Singh, J. Tian, K. Mamtani, J. King, J. T. Miller and U. S. Ozkan, *J. Catal.*, 2014, **317**, 30.
34 J. Sanetuntikul and S. Shanmugam, *Nanoscale*, 2015, 7644.
35 Y. Wang, A. Kong, X. Chen, Q. Lin and P. Feng, *ACS Catal.*, 2015, 3887.
36 M. Wang, W. Yang, H. Wang, C. Chen, Z.-Y. Zhou and S.-G. Sun, *ACS Catal.*, 2014, **4**, 3928.
37 B. Avasarala, R. Moore and P. Haldar, *Electrochim. Acta*, 2010, **55**, 4765.
38 K. Artyushkova, D. Habel-Rodriguez, T. S. Olson and P. Atanassov, *J. Power Sources*, 2013, **226**, 112.
39 S. Stariha, K. Artyushkova, A. Serov and P. Atanassov, *Int. J. Hydrogen Energy*, 2015, 1.
40 Y. Nabae, M. Sonoda, C. Yamauchi, Y. Hosaka, A. Isoda and T. Aoki, *Catal. Sci. Technol.*, 2014, **4**, 1400.
41 Y. Hu, J. O. Jensen, W. Zhang, S. Martin, R. Chenitz, C. Pan, W. Xing, N. J. Bjerrum and Q. Li, *J. Mater. Chem. A*, 2015, **3**, 1752.

Graphical Abstract

Effect of Pyrolysis Pressure on Activity of Fe-N-C Catalysts for Oxygen Reduction

In the synthesis of Fe-N-C catalysts by high-pressure pyrolysis, higher precursor loading increases gas-phase pressure and enhances nitrogen retention, active site density and ORR activity.